Electronic states in a quantum lens

Arezky H. Rodríguez,[1] C. Trallero-Giner,[1] S. E. Ulloa,[2,3] and J. Marín-Antuña[1]
[1]*Department of Theoretical Physics, University of Havana, 10400, Havana, Cuba*
[2]*Department of Physics and Astronomy, Ohio University, Athens, Ohio 45701-2979*
[3]*Condensed Matter and Surface Sciences Program, Ohio University, Athens, Ohio 45701-2979*
(Received 18 July 2000; published 12 March 2001)

We present a model to find analytically the electronic states in self-assembled quantum dots with a truncated spherical cap (''lens'') geometry. A conformal analytical image is designed to map the quantum dot boundary into a dot with semispherical shape. The Hamiltonian for a carrier confined in the quantum lens is correspondingly mapped into an equivalent operator and its eigenvalues and eigenfunctions for the corresponding Dirichlet problem are analyzed. A modified Rayleigh-Schrödinger perturbation theory is presented to obtain analytical expressions for the energy levels and wave functions as a function of the spherical cap height b and radius a of the circular cross section. Calculations for a hard wall confinement potential are presented, and the effect of decreasing symmetry on the energy values and eigenfunctions of the lens-shape quantum dot is studied. As the degeneracies of a semicircular geometry are broken for $b \neq a$, our perturbation approach allows tracking of the split states. Energy states and electronic wave functions with $m=0$ present the most pronounced influence on the reduction of the lens height. The method and expressions presented here can be straightforwardly extended to deal with more general Hamiltonians, including strains and valence-band coupling effects in Group III–V and Group II–VI self-assembled quantum dots.

DOI: 10.1103/PhysRevB.63.125319 PACS number(s): 73.61.−r, 73.21.−b, 03.65.Ge, 78.30.Fs

I. INTRODUCTION

Quantum dots obtained by interrupted growth in strained semiconductor interfaces are currently under intense study by many experimental and theoretical groups.[1] These ''self-assembled'' quantum dots are mostly dislocation free, coherent islands of deposited material on the surface of a different semiconductor. The lattice mismatch from one semiconductor to the other forces the segregation of material whenever the epitaxial growth exceeds a critical layer thickness, resulting in the growth of these so-called Stranski-Krastanov islands.[2] Deposition of material past a critical thickness, which depends on the two materials used, results in large arrays of small islands with a rather narrow size distribution (with size variations well under 10%), and typically arranged randomly on the plane (although avoiding overlapping islands, for the most part).[1] More recently, some groups are working at producing in-plane ordering of islands following different approaches, including ''nucleation site engineering'' to favor certain locations for self-assembled dot growth.[3] These self-assembled quantum dots have, for the most part, a large area-to-height aspect ratio. In the case of InAs islands grown on a GaAs surface, the in-plane diameters are typically less than 30 nm, while their heights are below 10 nm.[4] Different techniques used to study the shape and size of these dots suggest, although not without some controversy, that the InGa/GaAs self-assembled quantum dots are lens shaped,[5–8] characterized by a spherical cap shape with circular cross section. Upon optical or other mechanisms of carrier injection, both electrons or holes have bound well-confined states inside these dots.

In fact, optical experiments on self-assembled dots demonstrate that these structures provide strong carrier confinement, as decreasing dot size produces strong blueshift of the extremely narrow luminescence peaks in *isolated* dots.[9–13] Confinement effects have also been shown to appear in magnetocapacitance and infrared absorption experiments by several groups.[14–17] Clear evidence of electronic shell states and their different degeneracies has been reported recently,[18] and applications such as storage of photoluminescence signals was demonstrated recently in gate-activated ''optical memories.''[19]

Simplifying the symmetry of the lens as a two-dimensional harmonic oscillator has been suggested to characterize the level structure for charge carriers in the dots, and this has proven useful in the interpretation of experiments.[20] Nevertheless, as we will show here, a lens geometry has quite a different level structure and wave functions with subtle symmetries, which might be seen in experiments. For example, we find that as the height of the cap or lens decreases, there is a larger shift of the wave function towards the plane of the lens (in comparison with the situation in a semispherical geometry). This shift becomes stronger for ''flatter'' lenses, and may even give rise to deconfinement of the state towards the substrate, for finite confinement potential, changing significantly the oscillator strength of electron-hole transitions, for example.[21] However, even before that occurs, the smaller height lens geometries exhibit a different level structure than the harmonic oscillator, as we show below. This structure may give rise to different Pauli blocking effects and transition rules, topics which are the subject of interest in recent experiments.[22]

In this paper we rigorously show that a complete set of wave functions can be generated with the correct lens symmetry, and used to describe the physical properties given by the differential equation of interest. For the sake of simplicity, we have applied our calculation here to the single-particle Schrödinger equation. The incorporation of nonpara-

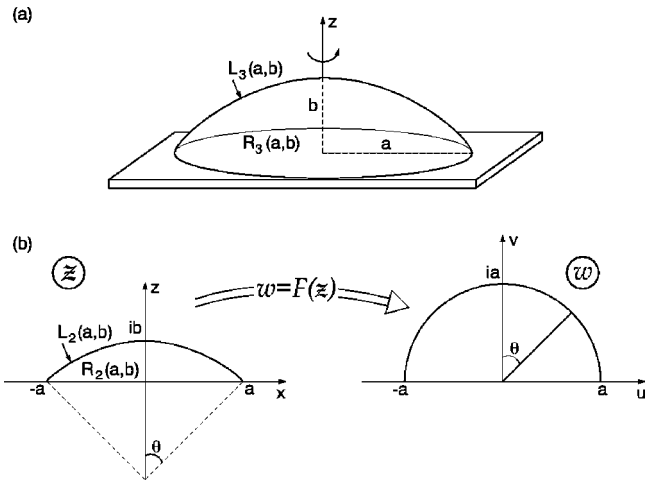

FIG. 1. (a) Lens cap of height b and radius a. (b) Conformal mapping from $\mathcal{Z}$ to $\mathcal{W}$.

bolic band dispersion or many-particle interactions is straightforward (if only a bit cumbersome). Although it is well known that strain effects are determinant in the description level structure of realistic self-assembled quantum dots,[23] the scope of the present paper is focused on the simpler single-particle Schrödinger equation. This provides the simplest proof of the conformal analytical transformation approach, mapping the dot lens geometry into a semispherical boundary. Notice that while our calculation provides an analytical approach to the understanding of electronic states in these structures, it also provides an interesting example of a generalization of perturbation theory for the conformal-mapped differential operator arising from the Schrödinger equation in the material. Since the conformal transformation used to map the lens into the semispherical geometry is nontrivial, the resulting differential equation in the transformed space reflects that complexity. Fortunately, our perturbation approach is robust for the identified small parameter of the problem, as we will show.

The remainder of the paper is structured as follows: in Sec. II we introduce the problem of the spherical cap geometry, its semispherical limit, and the conformal map which connects the two shapes. In that section, we also describe the perturbation approach needed to carry out the solution of the appropriately mapped Schrödinger operator, and explore the orthonormalization conditions of the basis used in the description of the general problem. In Sec. III we present some examples of the eigenstates for varying lens size, and analyze their angular and radial distribution functions. Section IV presents some discussions and conclusions, while the appendix contains details of the expansion described in Sec. II.

II. DIRICHLET PROBLEM FOR A QUANTUM LENS: CONFORMAL MAPPING

The shape of the quantum lens in real $\boldsymbol{r}$ space is shown in Fig. 1(a). $R_3(a,b)$ denotes the domain of the lens with boundary in $\boldsymbol{r}$ space given by a spherical cap of height b and circular cross section with radius a. Assuming a carrier Hamiltonian model with isotropic band and effective mass m^*, the eigenvalue problem for a particle confined in the lens is described by the operator

$$\hat{H}=-\frac{\hbar^2}{2m^*}\nabla_{\boldsymbol{r}}^2;\quad \boldsymbol{r}\in R_3(a,b), \tag{1}$$

obeying the Dirichlet boundary condition $\psi=0$ for $\boldsymbol{r}\in L_3(a,b)$. $L_3(a,b)$ is the boundary of the $R_3(a,b)$ domain. The operator (1) presents axial symmetry and all functions defined on $R_3(a,b)$ have the property $\phi(\varphi)=\phi(\varphi+2\pi)$, where φ is the axial angle. Hence, the solution of Eq. (1) can be written as

$$\psi(\boldsymbol{r})=\tilde{f}(\boldsymbol{\rho})\frac{\mathbf{e}^{im\varphi}}{\sqrt{2\pi}};\quad m=0,\pm1,\pm2,\ldots, \tag{2}$$

where $\boldsymbol{\rho}$ is a two-dimensional (2D) vector. Correspondingly, the operator (1) is transformed into an eigenvalue problem for the function $f(\boldsymbol{\rho})=\sqrt{\rho\sin\theta}\tilde{f}(\boldsymbol{\rho})$,

$$\left[\nabla_{\boldsymbol{\rho}}^2+\left(k_o^2-\frac{m^2-1/4}{\rho^2\sin^2\theta}\right)\right]f(\boldsymbol{\rho})=0;\quad \boldsymbol{\rho}\in R_2(a,b), \tag{3}$$

where $k_o^2=2m^*E/\hbar^2$, E is the energy of the eigenfunction $f(\boldsymbol{\rho})$, θ is the polar angle, $\nabla_{\boldsymbol{\rho}}^2$ is expressed in circular coordinates, and $R_2(a,b)$ is the 2D domain with boundary $L_2(a,b)$ in the $\boldsymbol{\rho}$ space shown in Fig. 1(b). The Hilbert space where the operator (3) is defined corresponds to the set of functions $f(\boldsymbol{\rho})\in R_2(a,b)$ with boundary condition $f(\boldsymbol{\rho})=0$ on $L_2(a,b)$.

A. Semispherical quantum dot

For the case of $b=a$, the lens shape of Fig. 1(a) has semispherical symmetry. Hence, the Dirichlet problem in Eq. (3) reduces to the conditions $f(a,\theta)=0$, and $f(\rho,\pi/2)=0$. The set $\{f_i\}$ of eigenfunctions of Eq. (3) on the R_2 domain forms an orthonormal basis with functions, which in polar coordinates are given by products of the associate Legendre polynomials and Bessel functions,

$$f_{n,l}^{(0)}(\rho,\theta)=\sqrt{\sin\theta}\,\frac{P_l^{|m|}(\cos\theta)}{N_{l,m}}\,\frac{J_{l+1/2}[(\mu_n^{(l)}/a)\rho]}{N_B}, \tag{4}$$

with $l=0,1,2,\ldots$, and the condition $-l\leqslant m\leqslant l$. The normalization constants $N_{l,m}$ and N_B are as usual given by

$$N_{l,m}=\sqrt{\frac{1}{2l+1}\frac{(l+|m|)!}{(l-|m|)!}};\quad N_B=\frac{a}{\sqrt{2}}J'_{l+1/2}(\mu_n^{(l)}), \tag{5}$$

where J'_q is the derivative of the Bessel function J_q, and $\mu_n^{(p)}$ is the nth zero, $J_{p+1/2}(\mu_n^{(p)})=0$. The eigenvalues are given by $E_{n,l}=\hbar^2(\mu_n^{(l)})^2/(2m^*a^2)$, and the boundary condition $f^{(0)}(\rho,\theta=\pi/2)=0$ restricts the values of the quantum numbers l and m to fulfill the condition $|l-m|=odd$. Ac-

cording to this condition, the degeneracy of states $f^{(0)}_{n,l}$ for a given energy $E_{n,l}$ is equal to l and the ground state corresponds to $l=1$, $m=0$, and $n=1$.

B. Quantum lens

The quantum dot with lens shape corresponds to the more general case when $b<a$. Here, we need to fulfill Eq. (3) with the Dirichlet condition over the boundary $L_2(a,b)$. The wave functions $f^{(0)}_{n,l}$ given by Eq. (4) are not a solution for the general case, because the problem has no longer the semicircular symmetry in θ. The energy number n and angular momentum l are clearly no longer good quantum numbers when $b\neq a$ and the m degeneracy is broken. To obtain an analytical solution of the problem (3) it is convenient to make a conformal mapping to the circular cap with domain $R_2(a,a)$ and boundary $L_2(a,a)$. The mapping enables us to solve the Dirichlet problem for the operator given by Eq. (3) in a Hilbert space where an orthonormal basis $\{f_i\}$ is known. We transform the quantum lens domain and boundary into a dot with semispherical shape, so that the circular cap defined by the domain $\mathcal{Z}=x-iz\in R_2(a,b)$, transforms into the semicircular domain $\mathcal{W}=u-iv\in R_2(a,a)$. This is accomplished by the transformation [see Fig. 1(b)]

$$\mathcal{W}(\mathcal{Z})=\frac{2a}{1+[(a-\mathcal{Z})/(a+\mathcal{Z})]^{\alpha}}-a;\quad \alpha=\frac{\pi/4}{\arctan(b/a)}. \tag{6}$$

In the complex plane $\mathcal{W}$, we have the parameter equations: $u=\rho\sin\theta$, $v=\rho\cos\theta$, $0<\rho<a$, and $0<\theta<\pi/2$. The eigenvalue problem (3) is thus transformed by this conformal mapping into the problem

$$\nabla^2_{(u,v)}F(u,v)+\mathcal{J}_{\alpha}(u,v)\left(k^2-\frac{m^2-1/4}{\mathcal{X}^2_{\alpha}(u,v)}\right)F(u,v)=0;$$

$$(u,v)\in R_2(a,a), \tag{7}$$

with the boundary condition,

$$F(u,v)|_{(u,v)\in L_2(a,a)}=0. \tag{8}$$

The functions $\mathcal{J}_{\alpha}(u,v)=|\mathrm{d}\mathcal{Z}/\mathrm{d}\mathcal{W}|^2$ (the Jacobian) and $\mathcal{J}_{\alpha}/\mathcal{X}^2_{\alpha}$ are given in Appendix A, and are mathematical objects that contain the information of the lens geometry, where the subscript α is given in Eq. (6). It should be noted that $\alpha\geqslant 1$, since $b\leqslant a$, and for $\alpha=1$ the Jacobian $\mathcal{J}_{\alpha}$ reduces to 1, while $\mathcal{J}_{\alpha}/\mathcal{X}^2_{\alpha}$ reduces to $1/u^2=1/(\rho\sin\theta)^2$.

The Hilbert space on which the operator (7) is defined must fulfill the Dirichlet boundary conditions on a semicircular domain, as indicated in Eq. (8). Thus, the set of functions that fulfill the conditions for the Hilbert space defined through Eq. (8) are the functions $f^{(0)}_{n,l}$ given in Eq. (4), and represent a complete set of orthonormal eigenfunctions for the operator in Eq. (7). Hence, the general solution $F(u,v)$ for a given m is given in term of the set $\{f^{(0)}_{n,l}\}$ such that

$$F=\sum_{n,l} C_{n,l}\, f^{(0)}_{n,l}(\boldsymbol{\rho}), \tag{9}$$

where $\boldsymbol{\rho}=(\rho,\theta)$ is here the parametrization of (u,v), and the functions $f^{(0)}_{n,l}$ are restricted to the condition $|l-m|=odd$. The coefficients $C_{n,l}$ have to be determined to satisfy the full operator and different approaches can be employed to accomplish this (e.g., matrix diagonalization techniques). A perturbation procedure, allowing to obtain the eigenfunctions F and eigenvalues k^2, is described in Sec. II D below.

C. Orthogonality and completeness

Equation (7) can be cast in operator form as

$$\hat{\boldsymbol{K}}F=\mathcal{J}_{\alpha}k^2F, \tag{10}$$

where $\hat{\boldsymbol{K}}$ involves the Laplace operator, $-\nabla^2_{(u,v)}$, and the term $(m^2-1/4)\mathcal{J}_{\alpha}/\mathcal{X}^2_{\alpha}(u,v)$. Equation (10) is an eigenvalue problem for the dimensionless energies $k^2_N(m)$, where N is a generic label for the different eigenstates F_N of Eq. (10). Let us now suppose that N and M correspond to different eigenvalues of Eq. (10). From the above equation it follows that

$$F^*_M\hat{\boldsymbol{K}}F_N-F_N\hat{\boldsymbol{K}}^*F^*_M=\mathcal{J}_{\alpha}(k^2_N-k^2_M)F^*_MF_N. \tag{11}$$

Making the integration over $\boldsymbol{\rho}(u,v)$ in the $R_2(a,a)$ domain, we obtain that

$$\int_{R_2(a,a)}[-F^*_M\nabla^2_{(u,v)}F_N+F_N\nabla^2_{(u,v)}F^*_M]\mathrm{d}^2\rho = (k^2_N-k^2_M)\int_{R_2(a,a)}F^*_MF_N\mathcal{J}_{\alpha}\mathrm{d}^2\rho. \tag{12}$$

Integration by parts gives us

$$(k^2_N-k^2_M)\int_{R_2(a,a)}\mathcal{J}_{\alpha}F^*_MF_N\mathrm{d}^2\rho=(F_N\nabla F^*_M - F^*_M\nabla F_N)|_{(u,v)\in L_2(a,a)}, \tag{13}$$

which due to the boundary condition (8), it is reduced to

$$(k^2_N-k^2_M)\int_{R_2(a,a)}\mathcal{J}_{\alpha}F^*_MF_N\mathrm{d}^2\rho=0. \tag{14}$$

For $N\neq M$, condition (14) represents the orthogonality property of the eigenfunction set $\{F_N\}$, where $\mathcal{J}_{\alpha}$ is clearly the *weighting factor* of the eigenproblem (7). Moreover, the operator $\hat{\boldsymbol{K}}$ is Hermitian, ensuring that the solution of the present problem is described by means of a complete orthonormal basis of eigenfunctions $\{F_N\}$ obeying the condition

$$\int_{R_2(a,a)} \mathcal{J}_\alpha F_M^* F_N \mathrm{d}^2\rho = \delta_{N,M}. \tag{15}$$

D. Perturbation theory

The coefficients $C_{n,l}$ in Eq. (9) and the eigenvalues k^2 can be obtained by perturbation theory if $b \approx a$ $(\alpha \to 1)$. In this case, the lens cap represents a perturbation from the semispherical geometry. In other words, the operator (7) can be rewritten in the form

$$(H_o + H_p) F(u,v) = 0, \tag{16}$$

with

$$H_o(u,v) = \nabla^2_{(u,v)} + \left(k^2 - \frac{m^2 - 1/4}{u^2} \right), \tag{17}$$

$$H_p(u,v) = k^2[\mathcal{J}_\alpha(u,v) - 1] - (m^2 - 1/4)\left(\frac{\mathcal{J}_\alpha(u,v)}{\mathcal{X}^2_\alpha(u,v)} - \frac{1}{u^2} \right). \tag{18}$$

The operator H_p vanishes when $\alpha \to 1$ $(b \to a)$ and it can be considered as a small perturbation operator, when the height b is close to the radius a. The set $\{f^{(0)}_{n,l}\}$ given by Eq. (4) are the eigenfunctions of the Hamiltonian H_o in the $\mathcal{W}$ space and form an orthonormal basis on the $R_2(a,a)$ domain. In order to find the solution of Eq. (16) as a function of the ratio b/a, we will develop a modified Rayleigh-Schrödinger perturbation theory. We note that the perturbation Hamiltonian H_p depends on the eigenvalue k^2, and as such requires a somewhat different approach. Substituting Eq. (9) in Eq. (16) we obtain

$$[(k^2 - k_o^2) + \langle n,l|H_p(k^2)|n,l\rangle] C_{n,l} + \sum_{n',l' \neq n,l} \langle n,l|H_p(k^2)|n',l'\rangle C_{n',l'} = 0. \tag{19}$$

The states of H_o are degenerate on the quantum number m. Nevertheless, according to Eq. (2),

$$\langle n,l,m|H_p|n',l',m'\rangle = \langle n,l|H_p|n',l'\rangle \delta_{m,m'}, \tag{20}$$

so that the matrix elements are diagonal on m and we can develop a perturbation theory in the absence of degeneracy. We represent the coefficients $C_{n,l}$ and its eigenvalues k^2 in a power series of the small parameter $\lambda = \alpha^{-1} - 1$ (which arises naturally from the expressions in Appendix A). We obtain up to first order in λ an expression for the wave functions given by

$$F_{N,m}(\rho,\theta) = f^{(0)}_{n,l}(\rho,\theta) + \lambda \Bigg[-\frac{1}{2} \left\langle n,l \left| \left(\frac{\partial \mathcal{J}_\alpha}{\partial \lambda} \right)_{\lambda=0} \right| n,l \right\rangle \times f^{(0)}_{n,l}(\rho,\theta) + \sum_{n',l' \neq n,l} f^{(0)}_{n',l'}(\rho,\theta) \times \frac{1}{k_o^2(n',l') - k_o^2(n,l)} \times \left\langle n',l' \left| k_o^2(n,l) \left(\frac{\partial \mathcal{J}_\alpha}{\partial \lambda} \right)_{\lambda=0} - (m^2 - 1/4) \frac{\partial}{\partial \lambda} \left(\frac{\mathcal{J}_\alpha}{\mathcal{X}^2_\alpha} \right)_{\lambda=0} \right| n,l \right\rangle \Bigg]. \tag{21}$$

We find for the eigenvalues up to second order, that

$$k^2(N,m) = k_o^2(n,l) + \lambda k_1^2(N,m) + \lambda^2 k_2^2(N,m), \tag{22}$$

where

$$k_1^2(N,m) = -\left\langle n,l \left| k_o^2(n,l) \left(\frac{\partial \mathcal{J}_\alpha}{\partial \lambda} \right)_{\lambda=0} - (m^2 - 1/4) \frac{\partial}{\partial \lambda} \left(\frac{\mathcal{J}_\alpha}{\mathcal{X}^2_\alpha} \right)_{\lambda=0} \right| n,l \right\rangle, \tag{23}$$

$$k_2^2(N,m) = -\sum_{n',l' \neq n,l} \frac{\left\langle n',l' \left| k_o^2(n,l) \left(\frac{\partial \mathcal{J}_\alpha}{\partial \lambda} \right)_{\lambda=0} - (m^2 - 1/4) \frac{\partial}{\partial \lambda} \left(\frac{\mathcal{J}_\alpha}{\mathcal{X}^2_\alpha} \right)_{\lambda=0} \right| n,l \right\rangle^2}{k_o^2(n',l') - k_o^2(n,l)} - \frac{1}{2} \left\langle n,l \left| k_1^2(N,m) \left(\frac{\partial \mathcal{J}_\alpha}{\partial \lambda} \right)_{\lambda=0} + k_o^2(n,l) \times \left(\frac{\partial^2 \mathcal{J}_\alpha}{\partial \lambda^2} \right)_{\lambda=0} - (m^2 - 1/4) \frac{\partial^2}{\partial \lambda^2} \left(\frac{\mathcal{J}_\alpha}{\mathcal{X}^2_\alpha} \right)_{\lambda=0} \right| n,l \right\rangle. \tag{24}$$

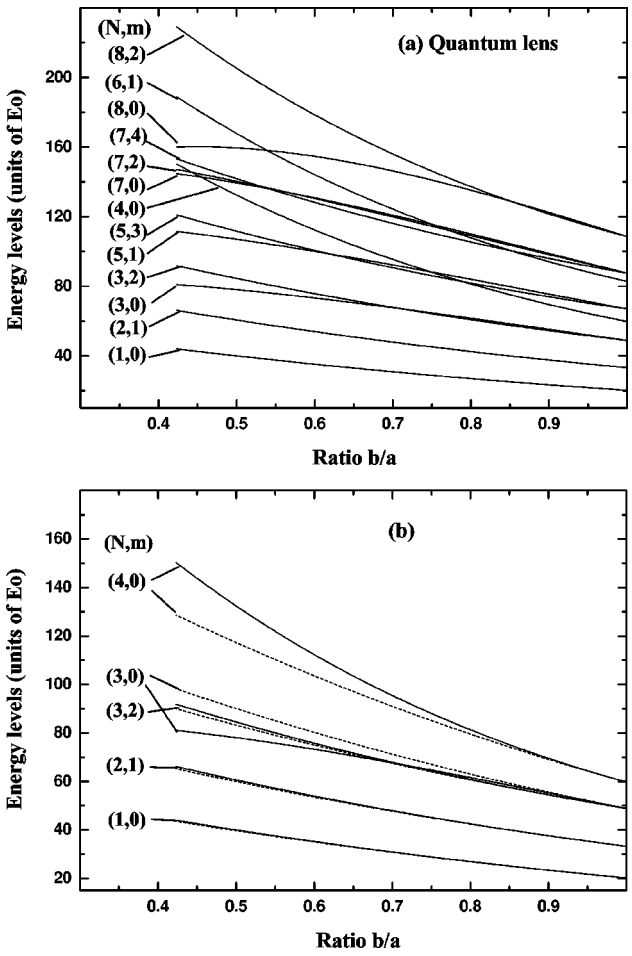

FIG. 2. Energy levels $E_{N,m}(b/a)$, labeled by (N,m), for a quantum lens as a function of the ratio b/a. The energies are given in units of $E_0=\hbar^2/(2m^*a^2)$. (a) The first 13 energy levels calculated up to second order in perturbation theory. (b) Comparison between results calculated up to first- (dotted lines) and second-order (solid) perturbation theory for the first five levels.

The different factors included in the geometric perturbation,

$$\left(\frac{\partial \mathcal{J}_\alpha}{\partial \lambda}\right)_{\lambda=0}, \left(\frac{\partial^2 \mathcal{J}_\alpha}{\partial \lambda^2}\right)_{\lambda=0}, \frac{\partial}{\partial \lambda}\left(\frac{\mathcal{J}_\alpha}{\mathcal{X}_\alpha^2}\right)_{\lambda=0}, \frac{\partial^2}{\partial \lambda^2}\left(\frac{\mathcal{J}_\alpha}{\mathcal{X}_\alpha^2}\right)_{\lambda=0} \tag{25}$$

are also given in Appendix A. In the framework of the infinite confinement model, the parameter dependence of Eqs. (21)–(24) is known, since the matrix elements play the role of constants and need to be evaluated only once. Note also that the above expressions are not the same as those found in a typical perturbation theory, as the difference arising in the k^2 term depends on the perturbation Hamiltonian H_p, which itself depends on the parameter λ.

III. THE EIGENVALUES AND WAVE FUNCTIONS

Figure 2(a) shows the first 13 energy levels in units of $E_o=\hbar^2/(2m^*a^2)$ for a quantum lens calculated by perturbation theory up to the second order in $\lambda=\alpha^{-1}-1$, as a function of the ratio b/a. The different eigenvalue curves are labeled by the quantum numbers (N,m). The semisphere case $(b/a=1)$ is indicated by the limiting value on the right vertical axis in each panel. One can see the breaking of degeneracy in the quantum number m, and the strong deviation from the semispherical case, as the ratio b/a decreases. The lower levels exhibit a weaker dependence on the decreasing b/a ratio, while the upper levels are strongly deviated from the semispherical case. In Fig. 2(b) the first five energy levels calculated up to first- (dotted lines) and second-order (solid lines) perturbation on the parameter λ are compared in the range $0.4\leqslant b/a\leqslant 1$. It can be seen that a strong deviation is present for the higher excited levels ($N=3$ and 4), while for $N=1$ and 2 the obtained results using Eq. (23) (first order perturbation theory) give a deviation smaller than 1% in comparison with those using Eq. (24) (second-order perturbation results). As a comparison, we calculate the absolute value for the electron ground-state energy E of an InAs quantum dot with $a=200$ Å and $m^*/m_o=0.023$. In the semispherical case one gets $E=83.3$ meV, while for the lens we obtain $E=96.9$, 108.8, and 128.7 meV, for $b/a=0.9$, 0.8, and 0.7, respectively. This variation of the lowest-energy values illustrates the strong influence of the lens geometry on the electronic levels.

The radial and angular probability density function in a given state N,m are defined as

$$P_{N,m}(\rho)=\int_0^{\pi/2}|F_{N,m}(\rho,\theta)|^2\rho \mathrm{d}\theta,$$

$$P_{N,m}(\theta)=\int_0^{a}|F_{N,m}(\rho,\theta)|^2\rho \mathrm{d}\rho. \tag{26}$$

The functions $P(\rho)$ and $P(\theta)$ are obtained up to first-order perturbation theory on λ according to the equations

$$P_{N,m}(\rho)=\rho\left(\frac{J_{l+1/2}(\mu_n^{(l)}\rho/a)}{N_B}\right)^2 \times\left\{1+\lambda\left[-\left\langle n,l\left|\left(\frac{\partial \mathcal{J}_\alpha}{\partial\lambda}\right)_{\lambda=0}\right|n,l\right\rangle + \int_0^{\pi/2}\mathrm{d}\theta\sin\theta\left(\frac{\partial \mathcal{J}_\alpha}{\partial\lambda}\right)_{\lambda=0}\left(\frac{P_l^{|m|}(\cos\theta)}{N_{l,m}}\right)^2\right]\right\};$$

$$\rho\in(0,a) \tag{27}$$

and

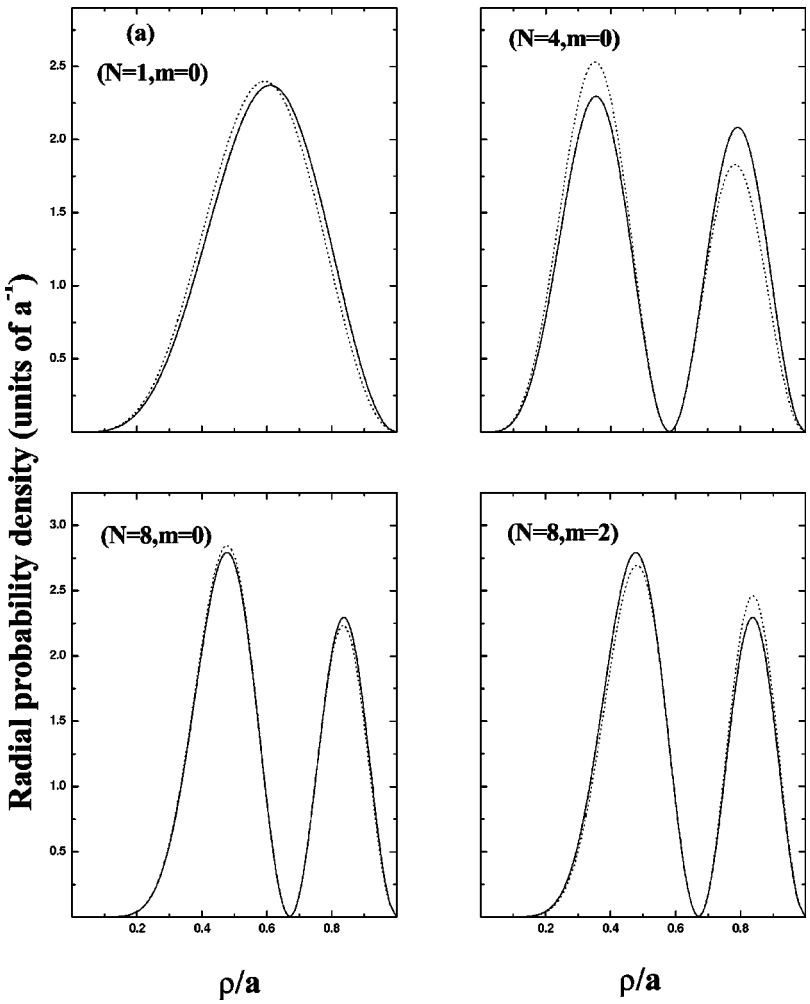

FIG. 3. (a) The radial probability density in a quantum lens $P_{N,m}(\rho)$, in units of a^{-1}, for different electronic states (N,m), and as function of the dimensionless coordinate $r=\rho/a$. (b) The angular probability density $P_{N,m}(\theta)$ as function of the angle θ. Two values of the ratio b/a are considered: $b/a=1$ (solid lines) and $b/a=0.509$ (dotted lines). The calculations were based on the perturbation theory described by Eqs. (27) and (28). Different states $(N,m)=(1,0)$, (4,0), (8,0), and (8,2) are indicated.

$$P_{N,m}(\theta)=\sin\theta\left(\frac{P_l^{|m|}(\cos\theta)}{N_{l,m}}\right)^2 \times\left\{1+\lambda\left[-\left\langle n,l\left|\left(\frac{\partial\mathcal{J}_\alpha}{\partial\lambda}\right)_{\lambda=0}\right|n,l\right\rangle + \int_0^a d\rho\,\rho\left(\frac{\partial\mathcal{J}_\alpha}{\partial\lambda}\right)_{\lambda=0}\left(\frac{J_{l+1/2}(\mu_n^{(l)}\rho/a)}{N_B}\right)^2\right]\right\};$$

$$\theta\in(0,\pi/2). \tag{28}$$

Figures 3(a) and 3(b) show the radial and angular probabilities given by Eqs. (27) and (28), respectively. In both cases the levels considered are $(N,m)=(1,0)$, (4,0), (8,0), and (8,2). Solid lines represent the semispherical case $(b/a=1)$, while the quantum cap with $b/a=0.509$ is shown by dotted lines, and illustrates the departure from the semispherical case for decreasing b/a ratio. In the case of the radial probability, the deviation observed when the ratio b/a decreases is relatively small, in comparison with the semispherical cap. In contrast, the angular probability shows a rather strong deviation as a function of b/a, as the maximum probability is shifted towards $\theta=\pi/2$, that is, the carrier is located more towards the plane $v=0$, as the cap height decreases [see Fig. 1(b)]. For all states, the maximum of $P(\rho)$ is smoothly shifted towards $\rho=0$, except for level (8,2). The different behavior observed for the radial and angular probability densities can be seen as arising from the fact that the geometry of the quantum dot is essentially decreasing in radius and not in angle, as b/a decreases. The radial probability is obtained by integration along the angle in all directions $(0<\theta<\pi/2)$, taking into account the angular contribution for a given ρ and certain geometry. On the other hand, the angular probability is calculated by taking the integration along the radius where the change of geometry is more important. Hence, one can say that the angular probability density $P(\theta)$ contains more information about the changing cap geometry than the function $P(\rho)$, as a function of b/a.

Finally, a test for the viability to obtain the wave functions and energies by the perturbation method, is given by the ratio between the matrix element of the perturbation Hamiltonian $\langle n,l|H_p(\mathcal{J}_\alpha,m)|n,l\rangle$ with respect to the nonperturbed dimensionless energy k_o^2,

$$\Delta_{N,m}\equiv\frac{|\langle n,l|H_p(\mathcal{J}_\alpha,m)|n,l\rangle|}{k_o^2(n,l)}. \tag{29}$$

The parameter $\Delta_{N,m}$ was calculated for the levels of Fig. 2 and is shown in Fig. 4 as a function of b/a. A necessary (but

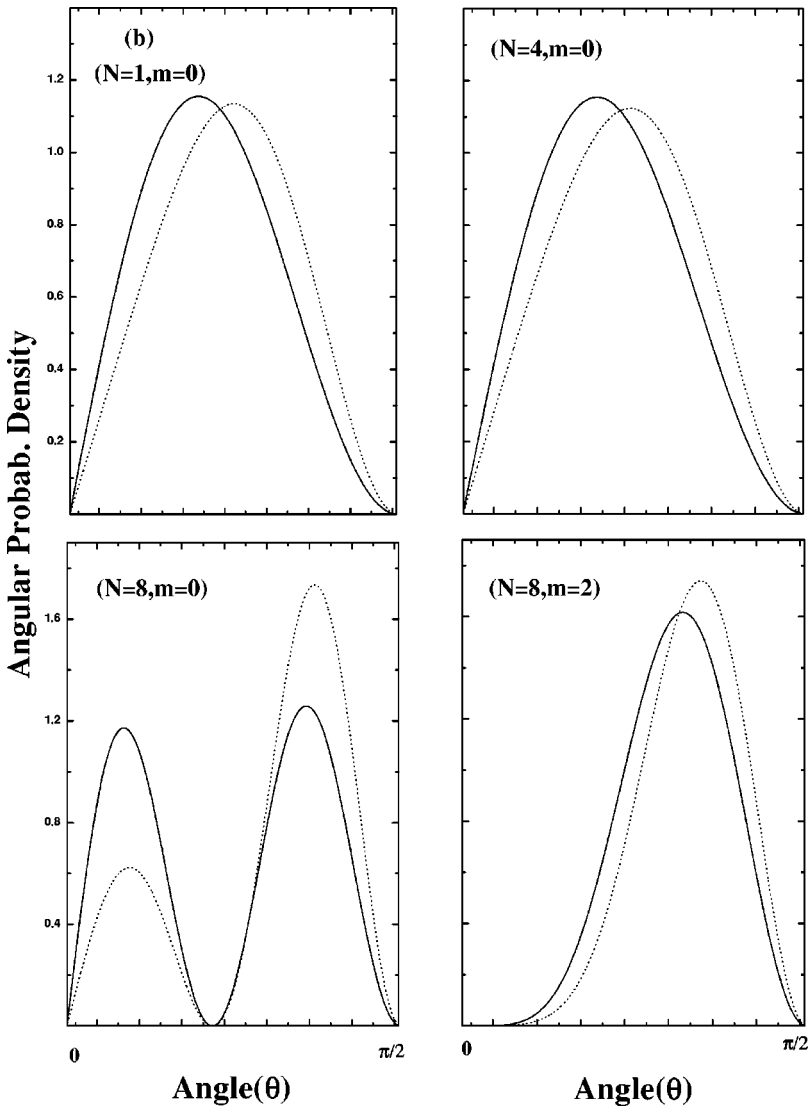

FIG. 3. (*Continued*).

not sufficient) condition for the perturbation theory to be valid is that $\Delta_{N,m}$ must be less than the unity, and this criterion is fulfilled for the range $0.4<b/a<1$. Another more restrictive condition for the applicability of this method is that $\langle n,l|H_p(\mathcal{J}_\alpha,m)|n',l'\rangle<|k_o^2(n,l)-k_o^2(n',l')|$, saying that the differences between nonperturbed dimensionless energy states need to be larger than the matrix elements of the perturbation. A more complete, nonperturbation, solution of Eq. (7) is needed to completely assess the validity of the perturbation approach. However, one can be confident that for small λ values, the eigenstates and eigenfunctions found represent an accurate solution to the problem, as the perturbation and the small parameter is well defined, and the procedure robust.

IV. CONCLUSIONS

We have presented a formal and systematic conformal analytical map model to describe quantum dots with lens geometry and circular cross section arising in the growth of low-dimensional semiconductor systems. The method can be directly extended to study 2D differential equations describing more realistic self-assembled quantum dots, which may include effects of band nonparabolicity, strain distributions, or other effects on the electronic levels of the lens. The reported transformation can be also extended straightforwardly to different physical models, such as phonon modes fulfilling their characteristic differential equations. The proposed conformal image maps the lens boundary into a dot with a semispherical shape, allowing one to obtain a complete set of orthonormal functions to characterize the physical problem keeping the full lens symmetry. We have applied the formalism to the eigenvalue and eigenfunction of the Schrödinger problem in a spherical cap geometry. The conformal mapping of the equation allows a modified but well-defined Rayleigh-Schrödinger perturbation approach, where the cap height to in-plane radius is used to define the small parameter of the theory.

We find that the wave functions are strongly shifted towards the flat face, as the height of the lens decreases, while the radial dependence is not affected as much. This change in the wave functions is interesting on its own, as it reflects the changes produced by the appropriate operator after the conformal mapping. Moreover, these changes may have impor-

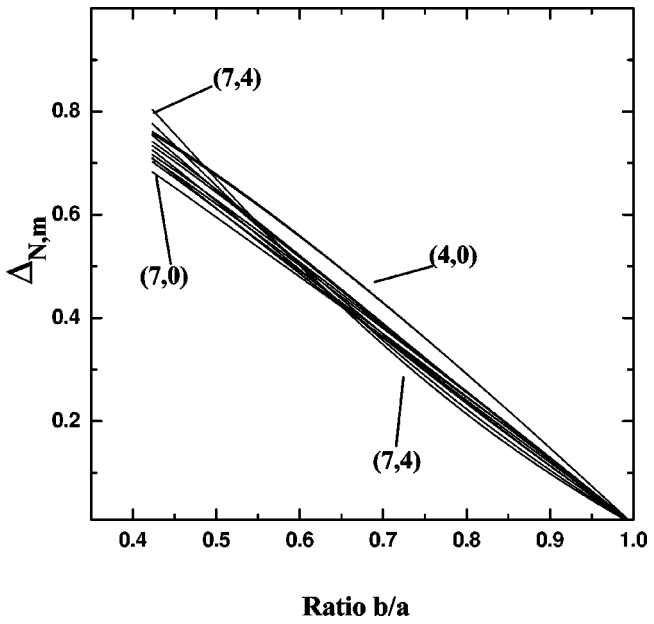

FIG. 4. Ratio between the matrix element and the energy $k_o^2(n,l)$ with respect to the ratio b/a of the quantum lens, Eq. (29). For all b/a between 0.4 and 1 the parameter Δ is small.

tant consequences for the different electronic and optical properties of self-assembled quantum dots. We are currently studying those properties and will report our findings in the future. The reported energy dependence on cap height to in-plane radius and semiconductors parameters can be useful to characterize the geometrical dimensions of these semiconductor nanostructures.

ACKNOWLEDGMENTS

SEU acknowledges partial support by the US DOE Grant No. DE-FG02-91ER45334.

APPENDIX A

The Jacobian of the transformation $\mathcal{W}(\mathcal{Z})$ is given by

$$\mathcal{J}_\alpha(r,\theta)=\frac{16(1/\alpha)^2}{R^{1-1/\alpha}[f_+^{1/\alpha}+f_-^{1/\alpha}+2R^{1/2\alpha}\cos(\phi/\alpha)]^2}, \tag{A1}$$

and the term $\mathcal{J}_\alpha/\mathcal{X}_\alpha^2$ can be cast as

$$\frac{\mathcal{J}_\alpha(r,\theta)}{\mathcal{X}_\alpha^2(r,\theta)}=\frac{16(1/\alpha)^2}{R^{1-1/\alpha}[f_+^{1/\alpha}-f_-^{1/\alpha}]^2}. \tag{A2}$$

In the above equations we have defined

$$r=\rho/a;\quad f_\pm=1+r^2\pm 2r\sin\theta;\quad R=f_+f_-, \tag{A3}$$

and

$$\phi=\begin{cases}\text{arctg}\left(\dfrac{2r\cos\theta}{1-r^2}\right); & r<1\\ \pi/2; & r=1.\end{cases} \tag{A4}$$

From Eqs. (A1) and (A2), it follows that

$$\mathcal{J}_{\alpha=1}(r,\theta)\equiv 1;\quad \left(\frac{\mathcal{J}_\alpha(r,\theta)}{\mathcal{X}_\alpha^2(r,\theta)}\right)_{\alpha=1}\equiv\frac{1}{r^2\sin^2\theta}, \tag{A5}$$

as one would expect.

Finally, the geometric perturbation factors in Eq. (25) are given by

$$\left(\frac{\partial\mathcal{J}_\alpha(r,\theta)}{\partial\lambda}\right)_{\lambda=0}=2-r\sin\theta\ln(f_+/f_-)+2\phi r\cos\theta, \tag{A6}$$

$$\frac{\partial}{\partial\lambda}\left(\frac{\mathcal{J}_\alpha(r,\theta)}{\mathcal{X}_\alpha^2(r,\theta)}\right)_{\lambda=0}=\frac{4r\sin\theta-(1+r^2)\ln(f_+/f_-)}{2r^3\sin^3\theta}, \tag{A7}$$

$$\left(\frac{\partial^2\mathcal{J}_\alpha(r,\theta)}{\partial\lambda^2}\right)_{\lambda=0}=\frac{1}{2}\left(\frac{\partial\mathcal{J}_\alpha}{\partial\lambda}\right)_{\lambda=0}\left[3\left(\frac{\partial\mathcal{J}_\alpha}{\partial\lambda}\right)_{\lambda=0}-8\right]-\frac{(1+r^2)}{4}\ln^2(f_+/f_-)+\phi^2(1-r^2)+2\ln^2R, \tag{A8}$$

$$\frac{\partial^2}{\partial\lambda^2}\left(\frac{\mathcal{J}_\alpha(r,\theta)}{\mathcal{X}_\alpha^2(r,\theta)}\right)_{\lambda=0}=\frac{(4r\sin\theta)^2-16r\sin\theta(1+r^2)\ln(f_+/f_-)}{8r^4\sin^4\theta}+\frac{[2(1+r^2)^2+R]\ln^2(f_+/f_-)}{8r^4\sin^4\theta}. \tag{A9}$$

[1] P. M. Petroff and G. Medeiros-Ribero, Mater. Res. Bull. **21**, 50 (1996).
[2] *Physics at Surfaces*, A. Zangwill (Cambridge University Press, Cambridge, 1988).
[3] H. Lee, J. A. Johnson, J. S. Speck, and P. M. Petroff, Appl. Phys. Lett. **78**, 105 (2000).
[4] D. Leonard, M. Krishnamurthy, C. M. Reaves, S. Denbaars, and P. M. Petroff, Appl. Phys. Lett. **63**, 3203 (1993); D. Leonard, K. Pond, and P. M. Petroff, Phys. Rev. B **50**, 11 687 (1994).
[5] D. J. Eaglesham and M. Cerullo, Phys. Rev. Lett. **64**, 1942 (1990).
[6] J. M. Moison, F. Houzay, F. Barthe, L. Leprince, E. Andre, and O. Vatel, Appl. Phys. Lett. **64**, 195 (1996).
[7] X. Z. Liao, J. Zou, X. F. Duan, D. J. H. Cockayne, R. Leon, and C. Lobo, Phys. Rev. B **58**, R4235 (1998).
[8] J. H. Zhu, K. Brunner, and G. Abstreiter, Appl. Phys. Lett. **72**, 424 (1998).
[9] S. Fafard, R. Leon, D. Leonard, J. L. Merz, and P. M. Petroff, Phys. Rev. B **50**, 8086 (1994).
[10] J.-Y. Marzin, J.-M. Gerard, A. Izrael, D. Barrier, and G. Bastard, Phys. Rev. Lett. **73**, 716 (1994).
[11] M. Grundmann, J. Christen, N. N. Ledentsov, J. Bohrer, D. Bimberg, S. S. Ruvimov, P. Werner, U. Richter, U. Gosele, J. Heydenreich, V. M. Ustinov, A. Yu. Egorov, A. E. Zhukov, P. S. Kop'ev, and Zh. I. Alferov, Phys. Rev. Lett. **74**, 4043 (1995).
[12] R. Leon, P. M. Petroff, D. Leonard, and S. Fafard, Science **267**, 1966 (1995).
[13] S. Lee, J. C. Kim, H. Rho, C. S. Kim, L. M. Smith, H. E. Jackson, J. K. Furdyna, and M. Dobrowolska, Phys. Rev. B **61**, R2405 (2000).
[14] H. Drexler, D. Leonard, W. Hansen, J. P. Kotthaus, and P. M. Petroff, Phys. Rev. Lett. **73**, 2252 (1994).
[15] M. Fricke, A. Lorke, J. P. Kotthaus, G. Medeiros-Ribeiro, and P. M. Petroff, Europhys. Lett. **36**, 197 (1996).
[16] G. Medeiros-Ribeiro, F. G. Pikus, P. M. Petroff, and A. L. Efros, Phys. Rev. B **55**, 1568 (1997).
[17] A. Lorke, R. J. Luyken, A. O. Govorov, J. P. Kotthaus, J. M. Garcia, and P. M. Petroff, Phys. Rev. Lett. **84**, 2223 (2000).
[18] B. T. Miller, W. Hansen, S. Manus, A. Lorke, and J. P. Kotthaus, Phys. Rev. B **56**, 6764 (1997).
[19] T. Lundstrom, W. S. Schoenfeld, H. Lee, and P. M. Petroff, Science **286**, 2312 (1999).
[20] M. Bayer, O. Stern, P. Hawrylak, S. Fafard, and A. Forchel, Nature (London) **405**, 923 (2000).
[21] See, for example, L. W. Wang, A. J. Williamson, A. Zunger, H. Jiang, and J. Singh, Appl. Phys. Lett. **76**, 339 (2000), and references therein.
[22] R. J. Warburton, C. Schäflein, D. Haft, F. Bickel, A. Lorke, K. Karrai, J. M. Garcia, W. Schoenfeld, and P. M. Petroff, Nature (London) **405**, 926 (2000).
[23] M. A. Causack, P. R. Briddon, and M. Jaros, Phys. Rev. B **56**, 4047 (1997).